Available online at www.sciencedirect.com
ScienceDirect
Journal of Magnetic Resonance 186 (2007) 282–292
JMR Journal of Magnetic Resonance
www.elsevier.com/locate/jmr

Quantitative discrimination of water and hydrocarbons in porous media by magnetization prepared centric-scan SPRITE

Linqing Li [a,b], Florin Marica [a], Quan Chen [a,1], Bryce MacMillan [a], Bruce J. Balcom [a,b,*]

[a] Department of Physics, MRI Centre, University of New Brunswick, Fredericton, New Brunswick, Canada E3B 5A3
[b] Department of Chemistry, P.O. Box 4400, University of New Brunswick, Fredericton, New Brunswick, Canada E3B 5A3

Received 14 August 2006; revised 25 February 2007
Available online 16 March 2007

Abstract

MRI has considerable potential as a non-destructive probe of porous media, offering the possibility of rapid quantification of local oil and water content. This potential has not yet, however, been completely realized. In this paper, we explore a general magnetization preparation approach to the discrimination of water and oil in a model, representative, porous medium. These measurements have, as a common element, a centric scan pure phase encode readout based on the SPRITE methodology. Magnetization preparation permits facile T_1, T_2 and diffusion coefficient mapping as the basis for oil and water discrimination. Diffusion coefficient mapping proved to be the most robust approach to discrimination of oil and water. These methods are illustrated through static experiments and a dynamic immiscible fluid displacement experiment.
© 2007 Elsevier Inc. All rights reserved.

Keywords: MRI; SPRITE; Centric scan; Magnetization preparation; Contrast imaging; Diffusion mapping; Immiscible oil displacement; Water flooding; Porous media; T_1 mapping; T_2 mapping; Pure phase encode

1. Introduction

Traditional experimental methods for the study of fluids in porous media are unable to resolve space. Often it is assumed that the porous media has an unknown but homogeneous structure. The volume and composition of fluids injected and recovered can be measured, but how the fluids are distributed and how they move inside the porous media can only be inferred [1]. X-ray computed tomography (CT) has allowed for determination of two-dimensional and three-dimensional rock structures, and in some cases fluid saturation and solute concentration in the sample. X-ray attenuation is, however, principally determined by the atomic number of the sample nuclei and is, therefore, dominated by the rock matrix. It is not well suited to observing fluids (water and oil have low atomic number) in the rock matrix. It is certainly not well suited to differentiating between these fluids except through the addition of high concentrations of contrast agents which will change the fluid properties [2].

MRI, however, has considerable potential as a non-destructive probe of porous media, offering the possibility of rapid quantification of oil and water content, spatially and temporally resolved, in a wide variety of media. Discrimination of water and oil in realistic porous media with MRI is important in many scientific fields such as petroleum engineering, the food industry, and environmental sciences [3–5].

To this point, the majority of MRI experiments for oil/water discrimination in porous media are designed such that only a single fluid phase is imaged. This is achieved either by doping the fluid phase with paramagnetic ions such as Cu^{2+}, Mn^{2+}, and Ni^{2+} [6–8], or by using deuterated

* Corresponding author. Address: Department of Physics, MRI Centre, University of New Brunswick, Fredericton, New Brunswick, Canada E3B 5A3. Fax: +1 506 453 4581.
E-mail address: bjb@unb.ca (B.J. Balcom).
[1] Present address: British Petroleum, Building 204, Sunbury-on-Thames, TW16 7LN, United Kingdom.

1090-7807/$ - see front matter © 2007 Elsevier Inc. All rights reserved.
doi:10.1016/j.jmr.2007.03.008

water, fluorinated oil or natural abundance ^{13}C oil as fluids [9–11]. However, the underlying relaxation time distributions of water and oil in the porous media, which may also be naturally short lived, makes the use of paramagnetic ions problematic. In addition, the high concentration of paramagnetic ions which may be required increases the risk of specific interactions between the paramagnetic ions and the porous media itself. The use of deuterated water or fluorinated oils are less attractive because of issues related to cost, safety and departure from natural conditions. ^{13}C due to its low natural abundance and reduced sensitivity, permits only limited applications [11,12].

It is more appealing to discriminate oil and water through magnetic resonance rather than through manipulation of the fluids themselves. A variety of MRI measurements, for example spin echo [13], inversion recovery [14], and chemical shift imaging [15], have been employed to discriminate oil and water in porous media. Each technique has distinct disadvantages. An underlying problem common to these methods is the assumption, which is not true in most realistic cases, that the spectral lines, or relaxation time distributions, of oil and water do not overlap.

Recent work by Hürlimann and Venkataramanan [16,17] has demonstrated the quantitative application of diffusion weighted protocols in grossly inhomogeneous B_0 and B_1 fields characteristic of oil-well logging tools. These methods are now sufficiently well understood that ''diffusion editing'' protocols may be considered a quantitative measurement for fixed magnetic field gradients. The experimental result is a two-dimensional plot of diffusivity D vs. T_2 [18]. First applications have been to the identification of different types of fluid in the rock (water, hydrocarbons, and drilling fluid filtrates) because of the typically strong diffusivity contrast. This technique suggests the potential application of diffusivity contrast to differentiate oil and water in porous media for quantitative MRI.

In this paper, we outline the use of an array of magnetization preparation methods incorporated into centric-scan SPRITE techniques [19], to acquire contrast images with either one fluid component suppressed or a series of images which permit mapping the two fluid components. With relaxation time preparation techniques, such as CPMG and inversion recovery, oil and water in porous media can not be discriminated quantitatively in the general case, due to distributions of the pertinent relaxation times.

However, by choosing proper diffusion contrast preparation, the diffusion coefficient can be used to spatially resolve and quantify oil and water content in porous media on a pixel by pixel basis. We apply this technique to quantitatively image an immiscible fluid displacement in a model porous medium. Such experiments will have direct relevance to the laboratory study of oil extraction from petroleum reservoirs and non-aqueous phase liquid (NAPL) remediation when applied to appropriate porous media.

2. Theory

2.1. Centric-scan SPRITE imaging technique

For centric-scan SPRITE techniques, data acquisition commences at the k-space origin and proceeds to the extremities of k-space. The local image intensity equation is

$$S = M(\rho_0, T_1, T_2, D)\exp(-\frac{t_p}{T_2^*})\sin\theta \quad (1)$$

$M(\rho_0, T_1, T_2, D)$ is the local sample magnetization, which is proportional to the local ^1H density, and the T_1, T_2, or diffusion coefficient according to the magnetization preparation scheme adopted for the experiments. Angle θ is the RF pulse flip angle, while T_2^* is the effective spin–spin relaxation time, and t_p is the phase encoding time.

The advantages of centric-scan SPRITE are profound: simplified image contrast is achieved, faster, with a better signal to noise ratio and a reduced gradient duty cycle compared to standard SPRITE [20].

The single exponential T_2^* decay feature for porous media is crucial to the quantitative nature of the experiment [21]. $M(\rho_0, T_1, T_2, D)$ imaging may be achieved for samples with short T_2^* by acquiring a series of centric-scan SPRITE images with different t_p, and then fitting to Eq. (1).

2.2. Magnetization preparation for centric-scan SPRITE

Perhaps the greatest attraction of MRI as an imaging modality lies in the flexibility of contrasts, which may be imposed upon the image. One possible way to apply contrast to an MR image is by ''preparation'' of the magnetization, separating the MR experiment (manipulating the sample magnetization related to molecular parameters) from the RF and gradient pulses associated with spatial resolution. This general idea is illustrated in Fig. 1a. At the beginning of a measurement the magnetization undergoes a sequence of RF and gradient pulses according to the desired contrast. The ''prepared'' signal is then stored along the z direction of magnetic field and spoil gradient pulses are applied to destroy residual transverse magnetization. Thereafter SPRITE can be applied in order to spatially resolve the contrast. The double half k-space (DHK) 1D [22] and spiral 2D SPRITE techniques are typical centric-scan SPRITE sequences, which have the advantages of pure phase encode centric scanning and are ideal ''readout' modules for prepared magnetization in material systems.

2.3. Magnetization preparation methods

2.3.1. T_1 and T_2 magnetization preparation

The inversion recovery experiment for magnetization preparation is outlined in Fig. 1b. The spoil gradient pulses destroy any remaining transverse magnetization. The stored magnetization is spatially resolved by a centric-scan SPRITE sequence. The T_2 magnetization preparation

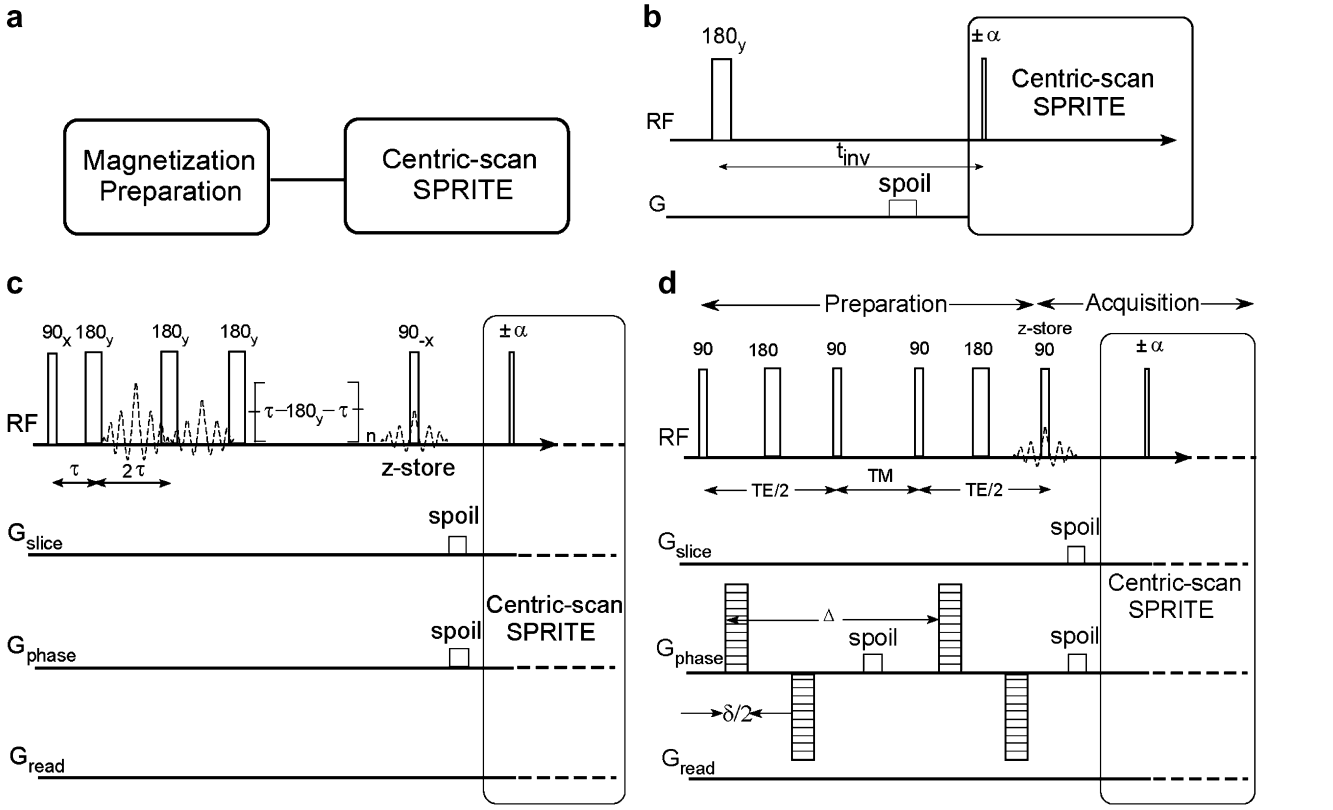

Fig. 1. Magnetization preparation with centric-scan SPRITE readout: (a) general schematic of the experiment; (b) inversion recovery sequence for T_1 mapping; (c) CPMG sequence for T_2 mapping; (d) pulsed field gradient stimulated echo (PFG-SE) with bipolar gradient pulses for diffusion mapping. The phase cycle of the PFGSE protocol, is based on the "13-interval, Condition 1" sequence of Cotts et al. [24].

experiment is displayed in Fig. 1c. At the end of the CPMG preparation, the sample magnetization is stored along the longitudinal direction and a spoil gradient pulse is followed by centric-scan SPRITE readout. We favor CPMG T_2 preparation with a short τ time to limit diffusion attenuation caused by molecular displacement through internal magnetic field gradients.

2.3.2. Pulsed field gradient stimulated echo (PFG-SE) preparation for diffusion weighted imaging

Stimulated echoes are advantageous with $T_1 \gg T_2$ system as, typically, encountered for fluids in porous media [23]. Background gradients associated with the medium itself, due to pore matrix susceptibility mismatch, may complicate a simple PFG diffusion measurement. We employ pulsed field gradients and stimulated echoes as suggested by Cotts [24]. This method eliminates contributions from the cross term ($g_0 g_a$) between the background gradient, g_0, and the applied gradient, g_a. The method is displayed in Fig. 1d. Two spoil gradients were used to eliminate the residual transverse magnetization after the two z-storage pulses. The observable attenuation including relaxation effects is given by the following equation

$$\ln\frac{I(g)}{I(0)} = -\gamma^2 g^2 \delta^2 D\left(\Delta - \frac{\delta}{3}\right) - \frac{\mathrm{TE}}{T_2} - \frac{\mathrm{TM}}{T_1} - \ln 2 \qquad (2)$$

where γ is the gyromagnetic ratio and $(\Delta - \delta/3)$ is the actual diffusion time with TE the echo time and TM the duration of the middle interval or mixing time. $I(0)$ refers to the initial intensity of the NMR signal.

2.3.3. Parameter optimization for magnetization preparation centric-scan SPRITE

In magnetization preparation centric-scan SPRITE images the acquisition parameters for the SPRITE readout are very important due to potentially significant M_z magnetization evolution during spatial encoding. M_z will evolve towards to a dynamic steady state, which bears no relation to the preparation, and may introduce contrast related artifacts in the final images. In order to maintain the desired resolution by controlling the level of blurring, the repetition time (TR), flip angle (α) and number of interleaves (N) must be carefully chosen. A set of general guidelines for the most appropriate choice of readout scheme, for given sample lifetimes, was systematically outlined by Khrapitchev [25].

2.4. Relaxation times and diffusion coefficients of fluids in porous media

For fluids confined in pores, the T_1 and T_2 value will be shorter than that of the bulk fluid if the fluid interacts with

the pore surface, which promotes MR relaxation. The relaxation times of fluids in porous media are determined by Eqs. (3) and (4), which are related to the sample pore size [26].

$$\frac{1}{T_1} = \rho_1 \frac{S}{V} \tag{3}$$

$$\frac{1}{T_2} = \rho_2 \frac{S}{V} \tag{4}$$

In Eqs. (3) and (4), ρ_1 is the spin–lattice surface relaxivity, ρ_2 is the spin–spin surface relaxivity, S/V is the pore surface-to-volume ratio. They form the basis of MR core analysis and well log interpretation, since the relaxation times T_1 or T_2 are therefore proportional to the pore size and a relaxation time distribution measurement is a useful proxy measurement for the pore size distribution.

The relaxation time distributions inherent to realistic porous media cause three difficulties in spatial quantification of water and oil in porous media. (1) Finite relaxation time weighted image data sets will not permit extraction of relaxation time distributions in reasonable image acquisition times, e.g. 8–16 images. There is insufficient data. (2) Overlap of the relaxation time distributions, which are commonly observed in bulk experiments, preclude their use in an imaging context to distinguish oil and water. (3) The relaxivity term $\rho_{1,2}$ in Eqs. (3) and (4) are determined by the matrix. Therefore, even in ideal cases where we might hope to approximate a bimodal relaxation time distribution with a bi-exponential decay, one has four experimental parameters which must be fit. If the lifetimes were already well characterized, i.e. they were matrix independent, fitting would be more reliable and robust.

Oil/water ratio determined through unrestricted fluid diffusion coefficient avoids all these problems. In the unrestricted diffusion limit, where the mean free path length is less than the pore size, the diffusion coefficient will be identical to that of the bulk fluid and may be readily determined from the literature, or simple calibration measurements. Since the results are essentially independent of the pore size distribution, in the case of water and model oils lacking a molecular size distribution, one anticipates a simple bi-exponential decay in sample magnetization with PFG diffusion contrast. This contrast may be resolved and quantified with the water and oil content the only two fitting parameters.

From the Einstein equation, $\langle r^2 \rangle = 2Dt$, where $\sqrt{\langle r^2 \rangle}$ is the diffusion distance, t is the diffusion evolution time, and D is the diffusion coefficient, we can determine the minimum pore size range for this approach. In the Cotts PFG sequence, the diffusion evolution time may readily be limited to 10 ms dependent on the maximum gradient used in the diffusion contrast experiment. This corresponds to a 6.8 μm diffusion distance for water. If a simpler PFG measurement were employed, the evolution time could be even smaller. The potential exists therefore to examine porous media with pore sizes as small as several micrometers. The pore size range of porous media characteristic of petroleum reservoir varies from 1 to 100 μm. We note that the diffusion imaging approach should work even in cases of restricted diffusion, but the diffusion coefficients must be fit parameters complicating the data analysis.

3. Results and discussion

3.1. Relaxation time contrast imaging experiments

3.1.1. Bulk relaxation time measurements

Bulk relaxation time measurements of oil and water in sand are reported in Table 1. The T_2^*, due to inhomogeneous broadening by the matrix is very similar for both fluids. Discrimination of oil/water by T_2^* decay mapping is not possible. Results from oil and water bearing samples measured simultaneously are reported in Table 2. The T_1 and T_2 relaxation time fits were limited to single or bi-exponential decays as appropriate to reflect the multiple fluids with limited data points from MRI measurements.

Bulk CPMG and Inversion recovery measurements of relaxation time distributions from component water/oil samples are reproduced in Figs.2a and 3a, respectively. The two peaks in Fig. 2a result from an overlap of short and long T_2 relaxation time components of oil and water revealed in Table 1. The single peak in Fig. 3a results from the overlap of the T_1 relaxation times of oil and water. It is impossible for us to differentiate water and oil from the Laplace transform plot even in such simple oil/water mixtures.

3.1.2. DHK 1D SPRITE image with T_2, T_1 weighting

We employ simple 1D imaging to evaluate the potential for relaxation time mapping to distinguish oil and water. We consider first T_2 mapping. The individual T_2 weighted images in Fig. 2b, correspond to different echoes. The T_2 decay curves of Fig. 2c and d were created by plotting the signal intensity decay from an arbitrarily chosen pixel in the oil/sand sample and in the water/sand sample. The image derived single exponential decays correspond to the average bi-exponential bulk measurements, 430 and 790 ms for water/sand sample and oil/sand sample, respectively. The relaxation time measurements in Table 2 show that one is unable to extract water/oil ratio from T_2 relaxation time weighted images with a limited number of data points.

The individual T_1 weighted images in Fig. 3b were acquired at different delay times after inversion. Magnetization recovery data, from arbitrary pixels in the oil/sand and water/sand samples are reproduced in Fig. 3c and d. The T_1 fitting results from Fig. 3c, Fig. 3d agree with the bulk measurements of Table 1, 3030 ms and 2670 ms for the water/sand sample and oil/sand sample, respectively. The relaxation time measurements in Table 2 show that one is unable to extract water/oil ratio from T_1 relaxation time weighted images with a limited number of data points.

Table 1
Diffusion coefficient and relaxation times for separated samples

Relaxation time/diffusion coefficient	T_2^*[c] (μs)	T_1[a] (ms)		T_2[b] (ms)		D[d] (m^2/s)
Water in sand	320	$T_1 = 2700$	100%	$T_2\,(1) = 135$ $T_2\,(2) = 720$	41% 59%	$2.2 \pm 0.2 * 10^{-9}$
PDMS in sand	280	$T_1 = 1860$	100%	$T_2\,(1) = 250$ $T_2\,(2) = 1010$	69% 31%	$2.1 \pm 0.2 * 10^{-10}$

[a] Inversion recovery measurement.
[b] CPMG measurement $\tau = 500$ μs, number of echoes 8192.
[c] Single exponential decay observed.
[d] $D_{water} = 2.0 \pm 0.1 * 10^{-9}$ m^2/s, $D_{PDMS} = 2.1 \pm 0.1 * 10^{-10}$ m^2/s, bulk measurement.

Table 2
Relaxation times for the combined samples

Relaxation time	T_2^*[c] (μs)	T_1[a] (ms)		T_2[b] (ms)	
Water in sand and PDMS in sand	—	$T_1\,(1) = 2610$ $T_1\,(2) = 270$	91% 8%	$T_2\,(1) = 105$ $T_2\,(2) = 700$	33% 67%

[a] Inversion recovery measurement.
[b] CPMG measurement $\tau = 500$ μs, number of echoes = 8192.
[c] The chemical shift different between PDMS and water introduces a beating which precludes simple T_2^* fitting. The individual line widths dominate over the chemical shift difference.

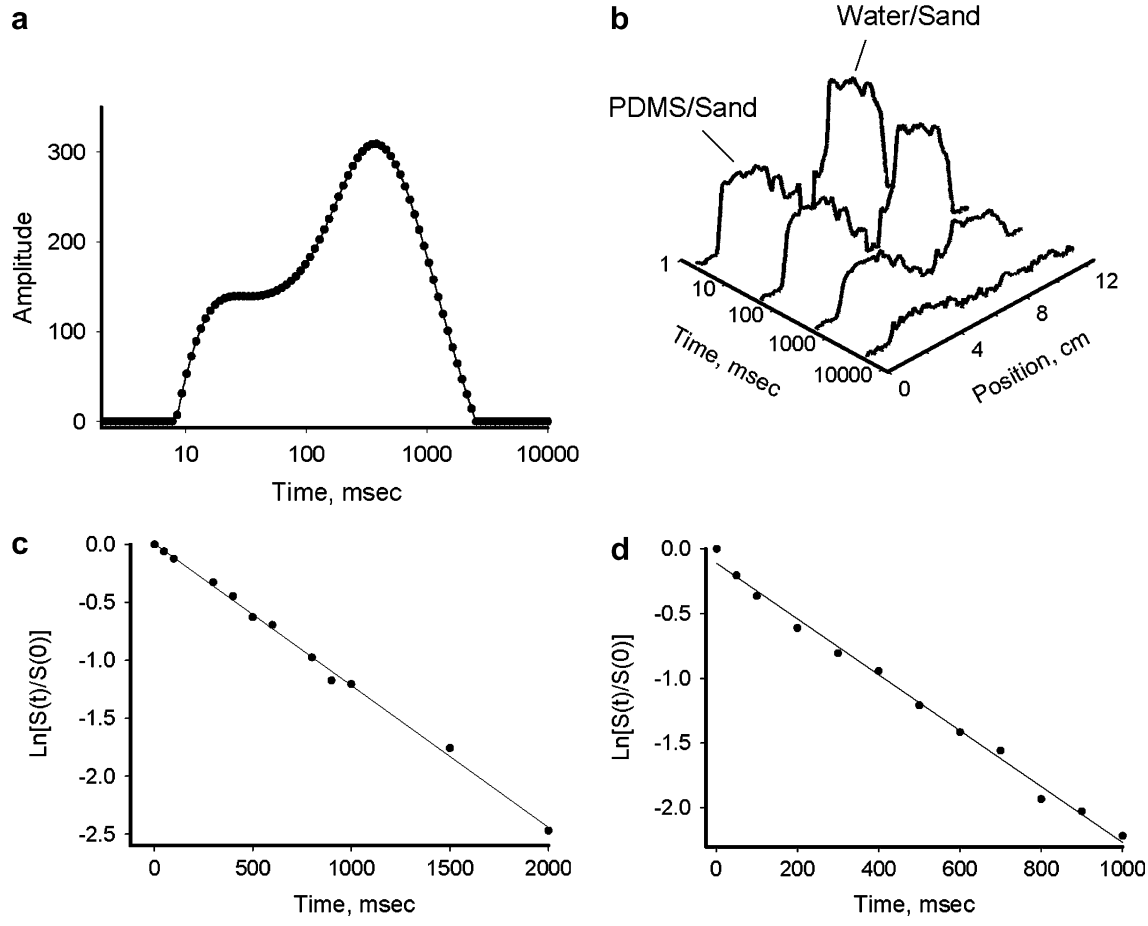

Fig. 2. (a) T_2 relaxation time distribution from Laplace transformation of bulk CPMG experiment data combined water/sand and oil/sand samples. (b) T_2 weighted 1D-DHK SPRITE images. Individual images correspond to echo times of 4, 50, 800, 6000 ms. Oil/sand sample is at left, while the water/sand sample is at right. (c) T_2 decay extracted from the oil/sand sample fits to a single exponential decay, $T_2 = 790$ ms; (d) T_2 decay extracted from the water/sand sample fits to a single exponential decay, $T_2 = 430$ ms.

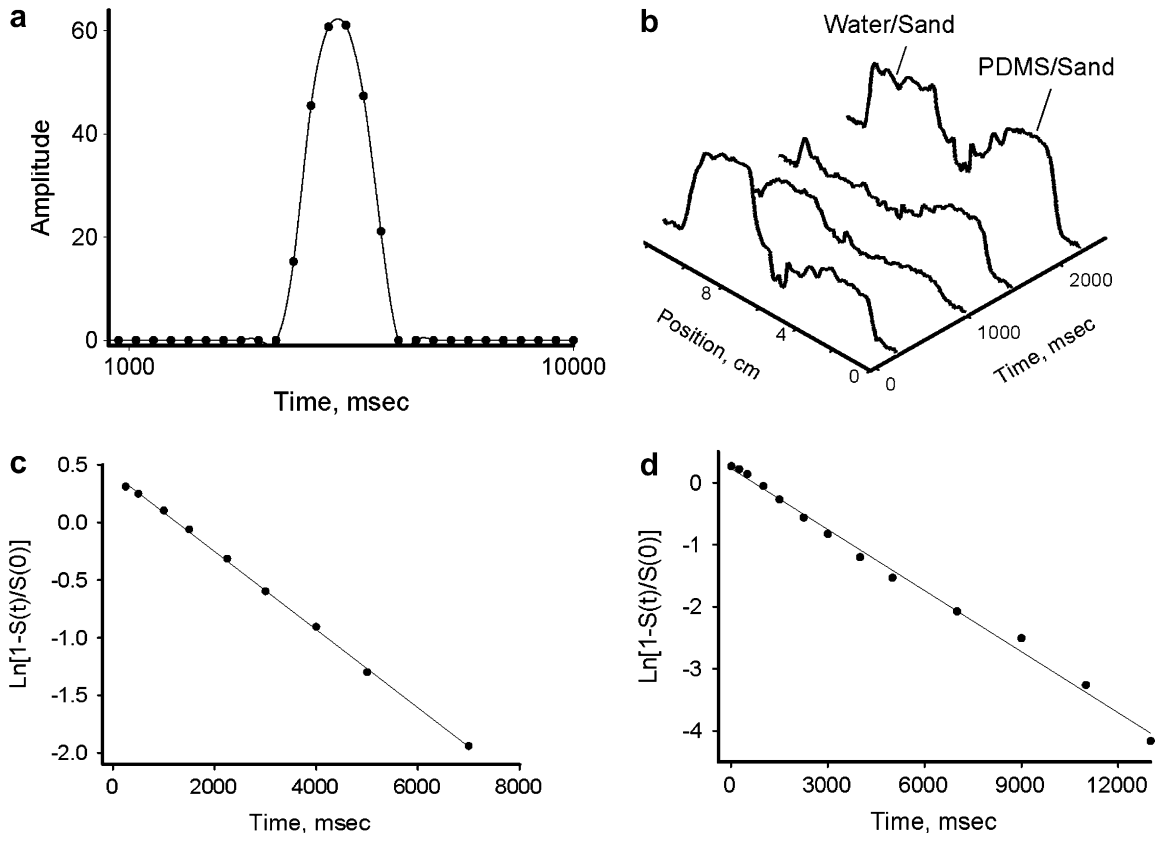

Fig. 3. (a) Relaxation time distribution from Laplace transformation of the bulk inversion recovery experiment data with combined water/sand and oil/sand samples. (b) Inversion recovery magnetization preparation for T_1 weighted 1D-DHK SPRITE images. Individual images correspond to delay time of 10, 500, 1000, and 3000 ms, respectively. The water/sand sample is at left, while the oil/sand sample is at right. (c) T_1 recovery curve extracted from the oil/sand sample fits to a single exponential decay, $T_1 = 2670$ ms; (d) T_1 recovery curve extracted from water/sand sample fits to a single exponential decay, $T_1 = 3030$ ms.

Two dimensional relaxation time maps (not shown) of similar samples yield identical conclusions to the one dimensional results presented.

3.1.3. DHK 1D SPRITE image with diffusion weighting

As outlined in Section 1 we anticipate a more robust and general quantification through the oil/water diffusion coefficients, providing the oil is reasonably viscous and the diffusion coefficients are different by at least a factor of 5.

In the diffusion weighted DHK 1D SPRITE experiments, the diffusion time ($\Delta = 20$ ms) was chosen in order to avoid restricted diffusion behavior. This diffusion evolution time corresponds to a 10 μm diffusion distance for water while the pore size of the sand used in this experiment was about 200 μm. Individual diffusion weighted images are reported in Fig. 4a. All images were acquired under different diffusion gradient amplitudes with the evolution time Δ fixed. The diffusion coefficients from the PDMS/sand and water/sand samples are obtained by fitting the log signal intensity from arbitrary pixels to a straight line. The fitting results in Fig. 4b, $1.9 \pm 0.2 * 10^{-9}$ and $2.4 \pm 0.2 * 10^{-10}$ m^2/s for the water/sand and oil/sand samples, respectively, agree with the bulk measurements in Table 1, and also agree with measurements of the pure liquid diffusion coefficients.

3.2. Centric-scan 2D SPRITE image with diffusion weighting

Centric-scan 2D sector SPRITE images with diffusion weighting, (diffusion time $\Delta = 20$ ms) of the water/sand and oil/sand samples are reproduced in Fig. 5. The only variable in the Fig. 5 image series is the amplitude of the diffusion gradient. The diffusion coefficient values in any pixel of oil/sand sample or water/sand sample can be obtained by fitting to Eq. (2). The results, $1.9 \pm 0.2 * 10^{-9}$ and $2.4 \pm 0.2 * 10^{-10}$ m^2/s for the water/sand and oil/sand samples, respectively, agree with the diffusion coefficients of the pure fluids and agree with the results of Section 3.1.3.

The superimposed oil/sand and water/sand samples were imaged in Fig. 6a. Fitting the diffusion decay series, Fig 6b, to extract the diffusion coefficient and relative water/oil ^{1}H amplitude yields diffusion coefficients of water/sand and oil/sand samples ($2.7 \pm 0.4 * 10^{-9}$ and $1.9 \pm 0.2 * 10^{-10}$ m^2/s, for oil and water, respectively) in good agreement with bulk measurement. The relative ^{1}H amplitude shows that water comprises 53% of the observed

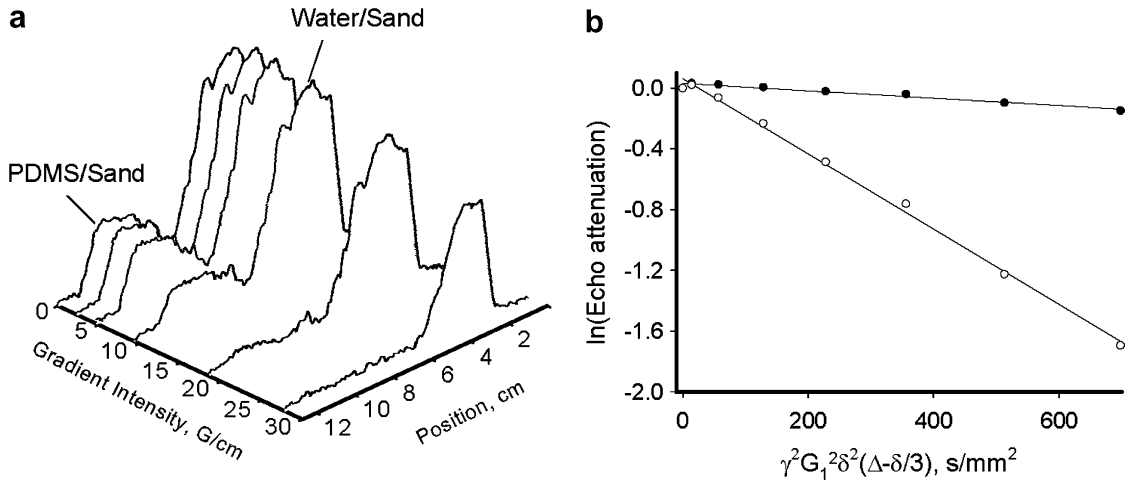

Fig. 4. (a) Pulsed field gradient stimulated echo (PFG-SE) preparation diffusion weighted 1D-DHK SPRITE images. Individual images had diffusion gradient pulse intensities of G_1 of 0, 2.5, 5, 10, 20 and 29 G/cm. The oil/sand sample is at left, while the water/sand sample is at right. (b) Diffusion decay of the oil/sand (●) and water/sand (○) samples, where $\delta = 5$ ms. The fitting results, $D_{\text{water in sand}} = 1.9 \pm 0.2 * 10^{-9}$ m^2/s ($D_{\text{water}} = 2.0 \pm 0.1 * 10^{-9}$ m^2/s for fluid) for the water/sand sample and $D_{\text{PDMS in sand}} = 2.4 \pm 0.2 * 10^{-10}$ m^2/s ($D_{\text{PDMS}} = 2.1 \pm 0.1 * 10^{-10}$ m^2/s for fluid) for the oil/sand sample.

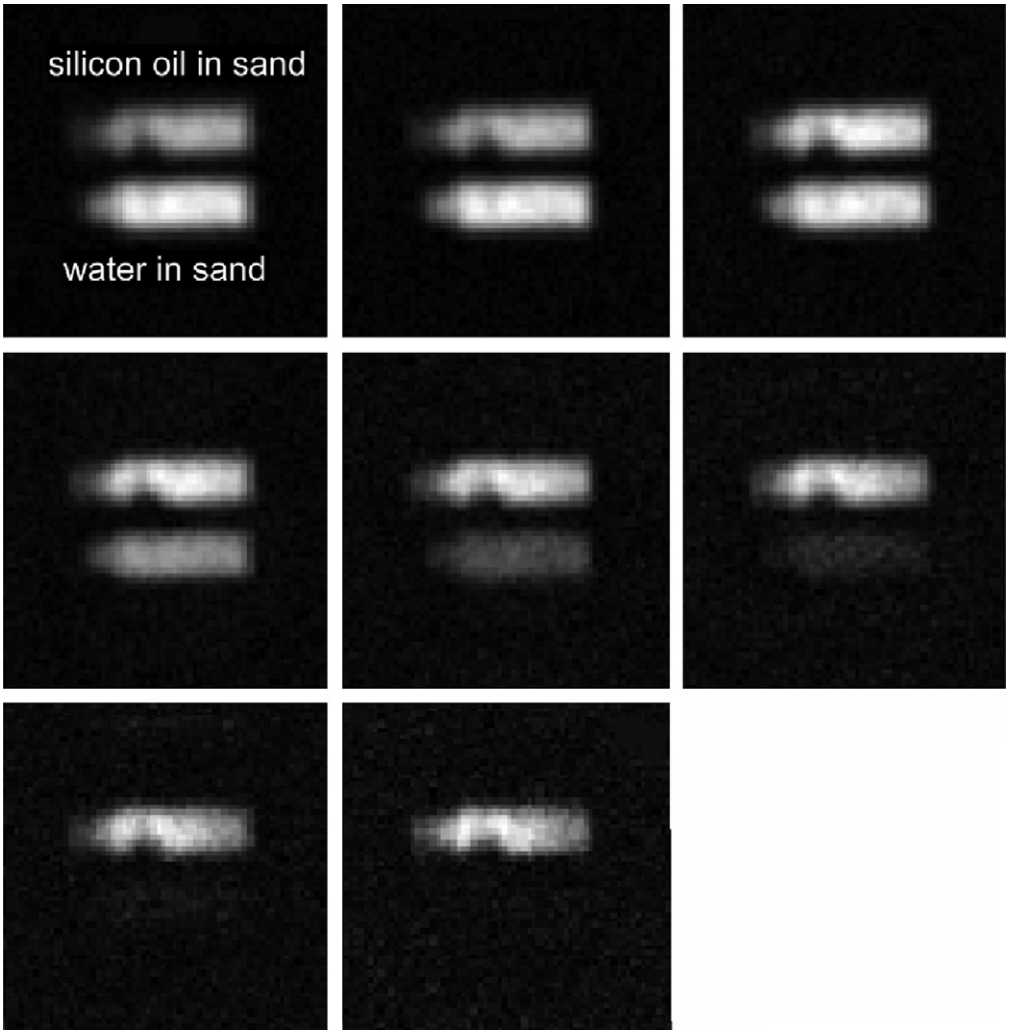

Fig. 5. Pulsed field gradient stimulated echo (PFG-SE) preparation for diffusion weighted 2D-SPRITE images. Individual images had diffusion gradient amplitudes of G_1 of 0, 4.3, 8.6, 12.9, 17.2, 21.5, 25.8, and 30.1 G/cm, respectively, with $\delta = 5$ ms; $\Delta = 20$ ms. With the diffusion gradient amplitude increasing, signal intensity of water in sand sample was greatly suppressed while there was not much suppression of the signal from the oil in sand sample. SNR for the first image is 10.

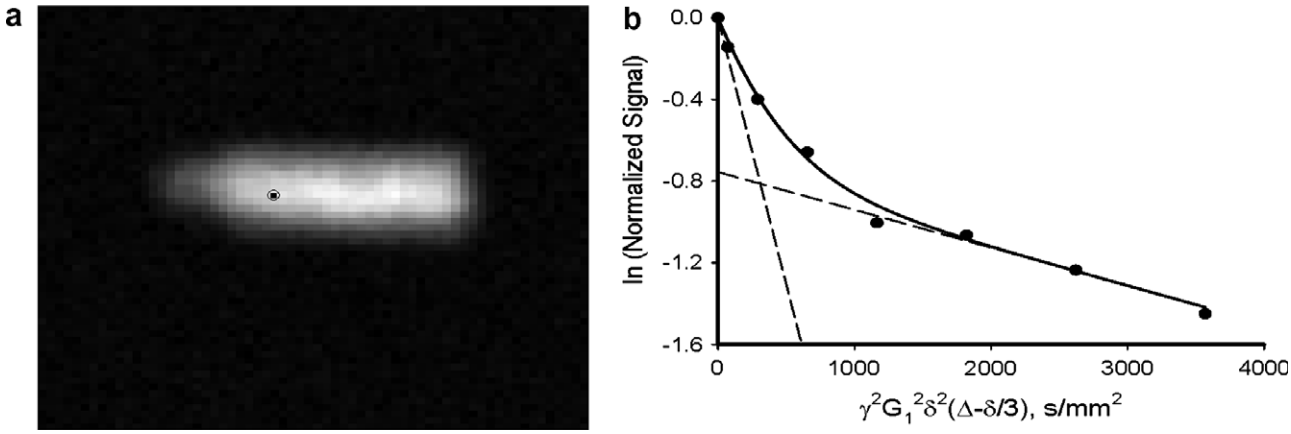

Fig. 6. (a) Diffusion weighted image of water/sand and oil/sand samples superimposed. SNR for the image is 7. (b) Data sets were exacted from images under different diffusion gradient amplitudes of G_1 of 0, 4.3, 8.6, 12.9, 17.2, 21.5, 25.8, and 30.1 G/cm, respectively, where $\delta = 5$ ms, $\Delta = 20$ ms. Fitting results are $D_{(\text{PDMS in sand})} = 1.9 \pm 0.2 * 10^{-10}$ m^2/s, 46% (bulk value, $D_{(\text{PDMS in sand})} = (2.1 \pm 0.1) * 10^{-10}$ m^2/s, 46.5%); $D_{(\text{water in sand})} = (2.7 \pm 0.4) * 10^{-9}$ m^2/s, 54% (bulk value, $D_{(\text{water in sand})} = 2.0 \pm 0.1 * 10^{-9}$ m^2/s, 53.5%). The data reveal that diffusion preparation may successfully discriminate oil and water in porous media.

image intensity while oil is 47%. This is also in reasonable agreement with the known sample proportions.

If we assume the bulk diffusion coefficients of water in sand and oil in sand as fixed input parameters in Eq. (2), determined from bulk measurement, the relative water/oil content is found to be 54% and 46%, respectively.

Simulation of Eq. (5) with variable ρ and realistic SNR shows that, even with limited data points, the oil/water

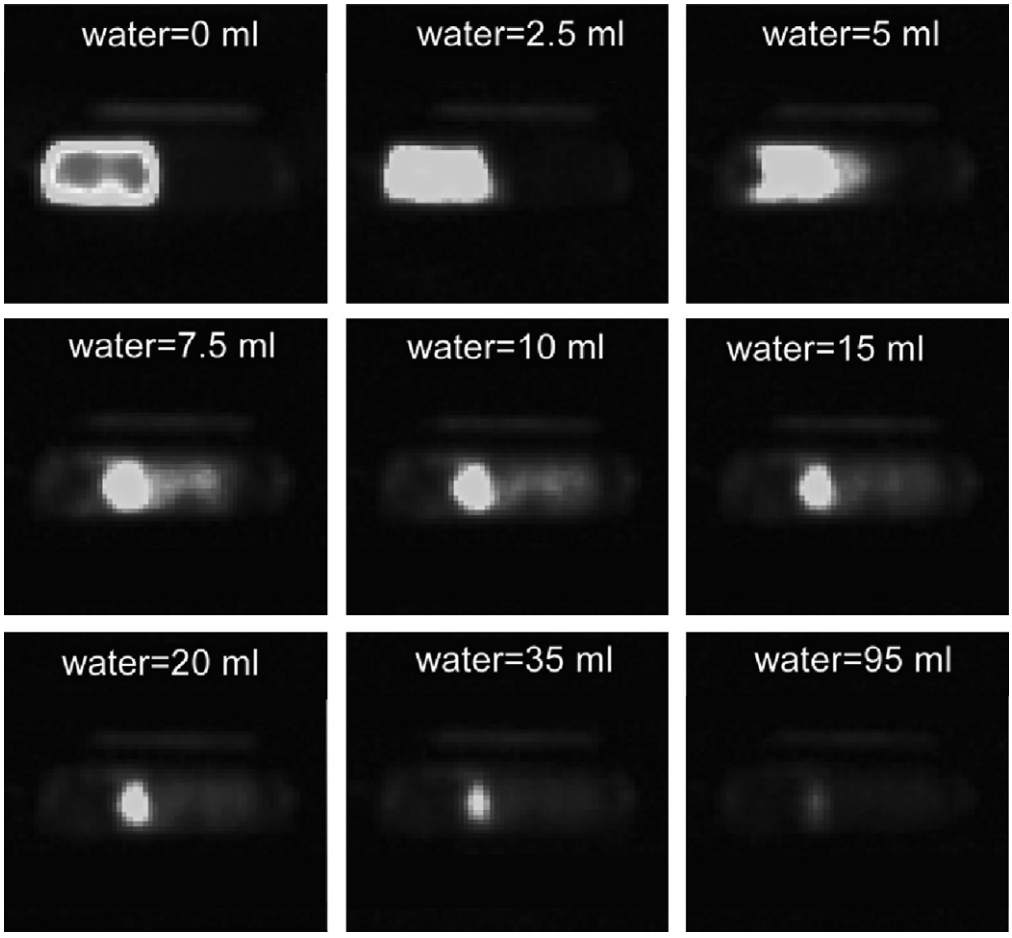

Fig. 7. Images acquired at different water flooding stages under the same diffusion gradient amplitude. Diffusion pulse parameters: $\delta = 5$ ms; $\Delta = 20$ ms; $G_1 = 29$ G/cm. Water is suppressed by diffusion PFG contrast. Oil response to water flooding can be quantitatively mapped. SNR for the first image is 20.

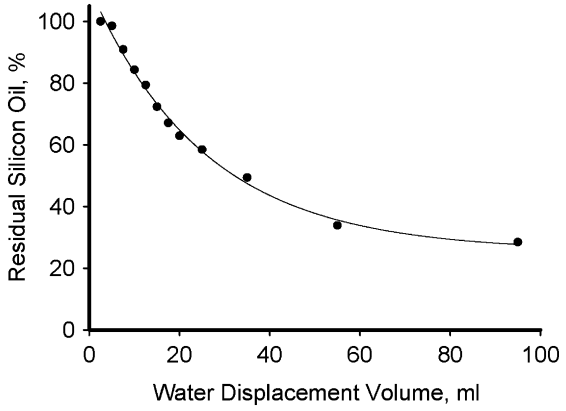

Fig. 8. Residual PDMS in matrix at different stages of water flooding. Each point was obtained by integrating and normalizing the signal intensity from individual images from Fig. 7. The water flow rate was maintained at 5 ml/min from 2.5 to 95 ml. However, the flow was interrupted for each image acquisition to ensure a quasi static sample. The oil disappearance is approximately exponential with water flooding volume down to less than 20% oil content.

determination is very robust when the diffusion coefficient values are known from control experiments and input to the equation. Relative water/oil ratios in the range of 10/1 to 1/10 may be extracted from appropriate MRI experiments, assuming diffusion coefficients which differ by more than a factor of 5 and SNR ratios of better than 10. These ideas will be further developed in a subsequent paper.

$$S = \rho_{0_1} e^{-bD_1} + \rho_{0_2} e^{-bD_2} \quad (5)$$

In Eq. (5), ρ_{01} and ρ_{02} are the spin densities of water and oil; D_1 and D_2 are the bulk diffusion coefficients of water and oil where $b = \gamma^2 g^2 \delta^2 (\Delta - \frac{\delta}{3})$.

Relaxation time weighted methods will fail in the general case to determine the oil and water content in porous media due to overlapping relaxation time distributions and the limited number of data points from the images.

Diffusion weighting, by contrast, was very successful in quantitative differentiation of oil and water in the sand matrix. The key feature is the well behaved bi-exponential decay of the observed image intensity with diffusion weighting. We believe the strategy may be successfully applied, in general, to a wide variety of realistic porous media.

3.3. Dynamic displacement of oil

3.3.1. Immiscible oil displacement by water flooding in sand

A quantitative description of immiscible oil displacement by water flooding in porous media is of fundamental importance for petroleum recovery [27]. The diffusion mapping idea was applied to a flooding experiment as a preliminary approach to quantitative oil distribution measurements in water flooding.

The magnetization preparation sequence of Fig. 1d was employed for oil/water displacement experiment. A diffusion mapping experiment was undertaken to determine reasonable diffusion gradient amplitudes to suppress the water signal with minimal attenuation of the oil signal. A diffusion gradient amplitude of 29 G/cm with an evolution time Δ of 20 ms gave 95% suppression of the water phase with only 30% suppression of oil. Images at different stages of water flooding are reproduced in Fig. 7. Displacement of the oil phase can be observed clearly from flooding stages of 0, 2.5, 5 ml. The overall displacement of the oil bolus and subsequent erosion is clearly observed on the image series.

The residual oil in sand, Fig. 8, is obtained by integrating and normalizing the signal intensity from each image in Fig. 7. The oil disappearance is approximately exponential with water flooding volume down to less than 20% oil content. We emphasize that although a simple diffusion weighting was employed in the image series of Fig. 7, it would be possible to fit for local water/oil content at each stage of the process by collecting the full range of diffusion weighted images.

The simple oil displacement imaging experiment shows that many fundamental features of enhanced oil recovery, such as entrapment, mobilization, breakup, and coalescence of oil ganglia, can be observed and quantified through laboratory scale experiments with the MRI methods developed in this work.

4. Conclusion

Magnetization preparation, especially diffusion weighting, combined with centric scan pure phase encoding readout based on the SPRITE methodology is an efficient method to discriminate oil and water in porous media.

The SPRITE MRI technique is specifically designed for short MR relaxation times and will work with T_2^* life times as short as tens of microseconds. The lower limit of T_2 values typically observed in relaxation time distribution measurements of core plugs [29], on the order of 1 ms, is substantially longer than this limit. It is true that T_2^* is reduced from the native T_2 by microscopic inhomogeneous broadening, however the extent of the reduction may be controlled by the choice of an appropriate static field strength.

Static 1D experiments were undertaken to discriminate macroscopically separated oil/sand and water/sand samples. The results show that while T_1 and T_2 preparation methods provide good contrast they are unable to quantitatively determine the oil/water content in porous media in general. However, diffusion contrast can be used as a quantitative imaging measurement to quantify local oil and water content in porous media.

A dynamic immiscible fluid displacement experiment was undertaken to further explore diffusion preparation for contrast and water/oil mapping. The residual oil in the solid matrix may be quantified from the contrast images. At any stage of flooding, the distribution and the oil/water content may be quantified from the diffusion images. Diffusion coefficient mapping, in the unrestricted diffusion limit, is the most robust approach to the discrimination of oil and water.

5. Experimental

All MRI measurements were performed on a MARAN spectrometer (Resonance Instruments Ltd., Oxford, UK) with a 7 T, widebore, horizontal superconducting magnet 7 T/60/AS (Magnex Scientific Ltd., Oxford, UK). The standard micro-imaging gradient set SGRAD156/100/S (Magnex Scientific Ltd., Oxford, UK) employed was powered by a set of three gradient amplifiers 7782 (AE Techron, Elkhart, USA), providing a maximum gradient strength of 38 G/cm. A home-made 62 mm inner diameter RF probe was used with an RF power amplifier 7T100S (Communication Power Corp., New York, USA). All measurement were carried out at 15 °C inside the probe.

The Acciss, Unifit, and Impstar processing packages developed in the IDL programming environment by the MRI Centre at UNB were used for image reconstruction, image fitting and image display. The WinDXP program was used for relaxation time distribution fitting.

Sand (Shaw Brick, Fredericton, NB, Canada) with a range of grain size 200–800μm diameter, porosity 0.41, void ratio 0.68, specific gravity 2.39, and estimated pore size 200 μm [28] was used in this study.

Poly(dimethylsiloxane), PDMS, silicon oil, with viscosity 4.56 cp and density 0.913 g/ml, (Aldrich Chemical Company, Inc, Milwaukee) and distilled water, with viscosity 1.139 cp at 15 °C were used in the T_2, T_1 and diffusion contrast experiments.

A constant rate, infusion/withdrawal, pump model 944 (Harvard Apparatus, Holliston, MA) was employed in the water flooding hydrocarbon experiments.

The static experiments employed two small vials, 45 mm in length and 15 mm in diameter. One vial was packed with sand saturated by 1.74 g water and the other one packed with sand saturated by 2.08 g PDMS. The relative ^{1}H ratio of water and oil was 53.5% and 46.5%, respectively.

Acquisition parameters for the DHK 1D-measurement in CPMG and inversion recovery magnetization preparation: Matrix 128, FOV = 120 mm, encoding time (t_p) = 100 μs, TR = 2 ms, flip angle = 10°, the delay between gradient interleaves was 6 s. Acquisition time = 16 s, number of scans = 4.

Acquisition parameters for DHK 1D-measurement in diffusion weighted magnetization preparation: Matrix 128, FOV = 100 mm, encoding time (t_p) = 100 μs, TR = 2 ms, flip angle = 10°, the delay between gradient interleaves was 3 s. Acquisition time = 17 s, number of scans = 16, diffusion steps = 8, from 0 to 34.2 G/cm.

Acquisition parameters for Sectoral-SPRITE 2D-measurement in diffusion weighted magnetization preparation: Matrix 64 * 64, interleaves = 8, FOV = 100 mm, encoding time (t_p) = 100 μs, TR = 2 ms, flip angle = 10°, The delay between gradient interleaves was 3 s. Acquisition time = 6 min, number of scan = 8, the phase cycle of the PFGSE protocol was based on the "13-interval, Condition 1" sequence of Cotts et al. [24].

In the water flooding experiments, a standard plastic 60 ml clinical syringe was cut into the sand holder, 8.5 cm in length, 2.8 cm in diameter. The left side (about 4.5 cm) was packed with sand saturated by 8.64 g (9.46 ml) PDMS. The right-hand side was packed with water (10.35 g) saturated sand. A pure PDMS tube was set above the sample holder as a reference. Water flooding was interrupted for 30–60 min at each measurement stage in order to acquire image data for water/oil mapping. Images were acquired after water flooding (flow rate = 5 ml/min) at overall volumes of 0, 2.5, 5, 7.5, 10, 12.5, 15, 17.5, 20, 25, 35, 55, and 95 ml of water, respectively.

Acknowledgments

The authors thank R.P. MacGregor and Alexandre A. Khrapitchev for their technical assistance and Yuesheng Cheng, A. Marble, and Ziheng Zhang of UNB as well as Drs Yiqiao Song and Martin Hurlimann of Schlumberger-Doll for useful suggestions. We also thank Dr. Murray Gingras from the University of Alberta for useful advice. B.J.B thanks NSERC of Canada, the Atlantic Innovation Fund, Petroleum Research Atlantic Canada, CFI and the Canada Chairs program for funding.

References

[1] A.C. Payatakes, Immiscible microdisplacement and ganglion dynamics in porous media, Rev. Chem. Eng. 2 (1984) 86–174.
[2] A. Kantzas, Recent advances in the characterization of porous media using computer assisted tomography of X-rays, CWLS J. 20 (1995) 99–102.
[3] S. Godefroy, J.-P. Korb, M. Fleury, Dynamics of water and oil at the solid–liquid interface in macroporous media and reservoir rocks, C. R. Acad. Sci. II fascicule c-chim. 4 (2001) 857–862.
[4] H. Hickey, M.B. MacMillan, B. Newling, M. Ramesh, P.V. Eijck, B.J. Balcom, Magnetic resonance relaxation measurements to determine oil and water content in fried foods, Food Res. Int. 39 (2006) 612–618.
[5] M. Pervizpour, S. Pamukcu, M. Horace, MRI of hydrocarbon-contaminated porous media, J. Comput. Civ. Eng. 13 (1999) 96–102.
[6] Y. Chu, C.J. Werth, A.J. Valocchi, H. Yoon, A.G. Webb, Magnetic resonance imaging of nonaqueous phase liquid during soil vapor extraction in heterogeneous porous media, J. Contam. Hydrol. 73 (2004) 15–37.
[7] Q. Chen, W. Kinzelbach, S. Oswald, Nuclear magnetic resonance imaging for studies of flow and transport in porous media, J. Environ. Qual. 31 (2002) 477–486.
[8] J. Chen, M.M. Dias, S. Patz, L.M. Schwartz, Magnetic resonance imaging of immiscible-fluid displacement in porous media, Phys. Rev. Lett. 61 (1988) 1489–1492.
[9] S. Chen, F. Qin, K.-H. Kim, A.T. Watson, NMR imaging of multiphase flow in porous media, AIChE J. 39 (1993) 925–934.
[10] D.A. Doughty, L. Tomutsa, Multinuclear NMR microscopy of two-phase fluid systems in porous rock, Magn. Reson. Imaging 14 (1996) 869–873.
[11] Y. Cheng, M.B. MacMillan, R.P. MacGregor, B.J. Balcom, Direct detection of hydrocarbon displacement in a model porous soil with NMR Imaging, Anal. Chem. 77 (2005) 1824–1830.
[12] Y. Cheng, Q. Huang, M. Eic, B.J. Balcom, CO_2 dynamic adsorption/adsorption on Zeolite 5A studied by ^{13}C magnetic resonance imaging, Langmuir 21 (2005) 4376–4381.

[13] M.L. Johns, L.F. Gladden, MRI study of non-aqueous phase liquid extraction from porous media, Magn. Reson. Imaging 16 (1998) 655–657.
[14] A.E. Fisher, B.J. Balcom, E.J. Forham, T.A. Carpent, L.D. Hall, A fast inversion recovery NMR imaging technique for mapping two-dimensional tracer diffusion and dispersion in heterogeneous media, J. Phys. D. Appl. Phys. 28 (1995) 384–397.
[15] S. Davies, A. Hardwick, D. Roberts, K. Spowage, K.J. Packer, Quantification of oil and water in preserved reservoir rock by NMR spectroscopy and image, Magn. Reson. Imaging 12 (1994) 349–353.
[16] M.D. Hürlimann, L. Venkataramanan, Quantitative measurement of two-dimensional distribution functions of diffusion and relaxation in grossly inhomogeneous fields, J. Magn. Reson. 157 (2002) 31–42.
[17] M.D. Hürlimann, Diffusion and relaxation effects in general stray field NMR experiments, J. Magn. Reson. 148 (2001) 367–378.
[18] L. Venkataramanan, Y.-Q. Song, M.D. Hürlimann, Solving Fredholm integrals of the first kind with tensor product structure in 2 and 2.5 dimensions, IEEE Trans. Signal Process 50 (2002) 1017–1026.
[19] I.V. Mastikhin, B.J. Balcom, P.J. Prado, C.B. Kennedy, SPRITE MRI with prepared magnetization and centric *k*-space sampling, J. Magn. Reson. 136 (1999) 159–168.
[20] M. Halse, D.J. Goodyear, M.B. MacMillan, P. Szomolanyi, D. Matheson, B.J. Balcom, Centric scan SPRITE magnetic resonance imaging, J. Magn. Reson. 165 (2003) 219–229.
[21] Q. Chen, A.E. Marble, B.G. Colpitts, B.J. Balcom, The internal magnetic field distribution, and single exponential magnetic resonance free induction decay, in rocks, J. Magn. Reson. 175 (2005) 300–308.
[22] K. Deka, M.B. MacMillan, A.V. Ouriadov, I.V. Mastikhin, J.J. Young, P.M. Glover, G.R. Ziegler, B.J. Balcom, Quantitative density profiling with pure phase encoding and a dedicated 1D gradient, J. Magn. Reson. 178 (2006) 25–32.
[23] D.L. Bihan, Diffusion and Perfusion Magnetic Resonance Imaging, Raven Press, New York, 1995.
[24] R.M. Cotts, M.J.R. Hoch, T. Sun, J.T. Marker, Pulsed field gradient stimulated echo methods for improved NMR diffusion measurements in heterogeneous systems, J. Magn. Reson. 83 (1989) 252–266.
[25] A.A. Khrapitchev, B. Newling, B.J. Balcom, Magnetization preparation for centric-scan SPRITE magnetic resonance imaging, J. Magn. Reson. 181 (2006) 271–279.
[26] R.L. Kleinberg, M.A. Horsfield, Transverse relaxation processes in porous sedimentary rock, J. Magn. Reson. 88 (1990) 9–19.
[27] N.P. Hankins, J.H. Harwell, Case studies for the feasibility of sweep improvement in surfactant-assisted waterflooding, J. Petrol. Sci. Eng. 17 (1997) 41–62.
[28] F.A.L. Dullien, Porous Media Fluid Transport and Pore Structure, Academic Press, New York, 1979, p. 95.
[29] Robert L. Kleinberg, Nuclear magnetic resonance, in: Po-zen Wong (Ed.), Chapter 9 in Methods in the Physics of Porous Media, Academic Press, New York, 1999, pp. 337–377.